International Journal of Engineering Applied Sciences and Technology, 2018
Vol. 3, Issue 4, ISSN No. 2455-2143, Pages 1-13
Published Online August 2018 in IJEAST (http://www.ijeast.com)

NUMERICAL SIMULATION OF THERMALLY DEVELOPING TURBULENT FLOW INSIDE A CIRCULAL TUBE

Ali Belhocine
Department of Mechanical Engineering
University of Sciences and Technology of Oran
L.P 1505 El -Mnaouer, USTO 31000 Oran (Algeria)

Oday Ibraheem Abdullah
System Technologies and Mechanical Design Methodology
Hamburg University of Technology
Hamburg Germany

Abstract— **A numerical study was conducted using the finite difference technique to examine the mechanism of energy transfer as well as turbulence in the case of turbulent flow fully developed in the channel with substantially constant wall temperature and constant heat flow conditions. The methodology of solving the thermal problem is based on the equation of energy for a fluid of constant properties by placing itself in the equilibrium hypothesis of an axisymmetric. The global equations and the initial and boundary conditions acting on the problem are configured in dimensionless form in order to predict the characteristics of the turbulent fluid flow inside the tube. Thus, using Thomas' algorithm, a program in FORTRAN version 95 was developed to numerically solve the discretized form of the system of equations describing the problem. Finally, using this elaborate program, we were able to simulate the flow characteristics, changing some parameters involved such as Reynolds number, the Prandtl number and the Peclet number, along the longitudinal coordinate to obtain important results of the thermal model. These are discussed in detail in this work. Comparisons between literatures correlation data and the calculated simulation indicate that the results are a good match to previously published quantities.**

Keywords— **Finite difference method, Nusselt number, fully developed turbulent flow, Reynolds number, flow pipe**

I. INTRODUCTION

Turbulent flow is a state of fluid moving in the direction of the flow guide, but with non-rectilinear trajectories. There will be trajectory crossings for all layers of fluid volume in motion which causes interactions between the fluid volumes and collisions on the walls of the flow guide. These collisions can cause noise. This type of flow is very hard to analyze. The modeling of turbulent fluid flows is an essential step for both mechanics and the field of engineering. We can meet them in various engineering applications, such as; sewage collection, drilling hydraulics, heat exchanger apparatus, treatment of polymer products and mineral oil, blood flow in the veins and arteries as well as other thermal applications with a very severe transfer rate. For the stationary case in a cylindrical tube, fully developed turbulent flows have been studied numerically by several authors using computer-based computation and simulation at different Reynolds numbers. These are to better understand the thermal problems are such flow. Several studies (Zhou *et al*.,2017; Wei *et al*.,2005; Everts & Meyer, (2018a, 2018b) ; Aravinth , 2000 ; Teitel & Antonia,1993; Koizumi, 2002) either digital or experiment on fully developed turbulent channel flows were conducted previously. Gnielinski (1973) developed equations describing both the fully developed region of the flow and the transition region through channels and pipes. These were then compared to experimental results for high Reynolds and Prandlt numbers. Correlations valid for the transient regime and the fully developed turbulent flow subjected to a uniform heat flux through a circular tube, have been developed in the work of Taler (2016) for Reynolds numbers Re, and Prandtl Pr and of which the number of Nusselt Nu is expressed as a function of the friction factor ξ (Re). Badus'haq (1993) carried out experiments through an electrically heated pipe in turbulent air flow to examine the local heat transfer characteristics in the steady state case. Belhocine and Wan Omar (2016), and Belhocine (2016) conducted a study to investigate the distribution of temperature in the pipes for a fully developed laminar flow. Recently, Belhocine and Wan Omar (2017) solved analytically the problem of convective heat transfer in a circular pipe whose solutions were in the form of the hypergeometric series. Belhocine and Wan Omar (2018) then used a similarity solution and Runge Kutta method in order to visualize analytically the thermal boundary layer in the vicinity of the inlet of the circular pipe.

In this paper , a two-dimensional heat transfer in a fully developed turbulent flow on circular duct are numerically investigated using a FORTRAN code which applied the finite difference method to solve the thermal problems on two boundary conditions, as it happens, constant wall temperature,

International Journal of Engineering Applied Sciences and Technology, 2018
Vol. 3, Issue 4, ISSN No. 2455-2143, Pages 1-13
Published Online August 2018 in IJEAST (http://www.ijeast.com)

and constant surface heat flux, and steady, axisymmetric flow. Finally, the numerical results of the model were validated by comparing them with some results available in the specialized literature. The comparisons give a good agreement with data from the literature..

II. THE FLOW GOVERNING EQUATIONS

The governing equations related to the flow are the continuity, momentum and energy equations:

$$\frac{\partial(\rho u_i)}{\partial x_i} = 0 \tag{1}$$

$$\frac{\partial}{\partial t}(\rho u_i) + \frac{\partial}{\partial x_j}(\rho u_i u_j) = -\frac{\partial P}{\partial x_i} + \frac{\partial}{\partial x_j}\left[\mu\left(\frac{\partial u_i}{\partial x_j} + \frac{\partial u_j}{\partial x_i} - \frac{2}{3}\delta_{ij}\frac{\partial u_j}{\partial x_i}\right)\right] + \frac{\partial}{\partial x_j}\left(-\rho\overline{u_i' u_j'}\right) \tag{2}$$

$$\frac{\partial}{\partial x_i}[u_i(\rho E + P)] = \frac{\partial}{\partial x_i}\left[\left(\lambda + \frac{c_p \mu_t}{Pr_t}\right)\frac{\partial T}{\partial x_j} + \mu\mu_t\left(\frac{\partial u_i}{\partial x_j} + \frac{\partial u_j}{\partial x_i} - \frac{2}{3}\delta_{ij}\frac{\partial u_j}{\partial x_i}\right)\right] \tag{3}$$

where λ is the thermal conductivity and E is the total energy, which can be expressed by

$$E = c_p T - P/\rho + u^2/2$$

From the momentum equation a transport equation for the Reynolds stress tensor can be derived (Bryant *et al.*, 2018) as;

$$\frac{\partial(\rho\overline{u_i' u_j'})}{\partial t} + C_{ij} = D_{T,ij} + D_{I,ij} + P_{ij} + \Phi_{ij} + \varepsilon_{ij} \tag{4}$$

Where C_{ij}, $D_{T,ij}$, $D_{I,ij}$, P_{ij} , Φ_{ij} and ε_{ij} are respectively the terms for convection , turbulent diffusion, molecular diffusion , shear stress production, stress-strain, and viscosity dissipation. These could be written as follows.

$$C_{ij} = \frac{\partial}{\partial x_k}(\rho\, u_k \overline{u_i' u_j'}) \tag{5}$$

$$D_{T,ij} = -\frac{\partial}{\partial x_k}(\rho\, \overline{u_i' u_j' u_k'} + \overline{P' u_i'}\delta_{kj} + \overline{P' u_j'}\delta_{ik}) \tag{6}$$

$$D_{I,ij} = \frac{\partial}{\partial x_k}\left[\mu\frac{\partial}{\partial x_k}(\overline{u_i' u_j'})\right] \tag{7}$$

$$P_{ij} = -\rho\left(\overline{u_i' u_k'}\frac{\partial u_j}{\partial x_k} + \overline{u_j' u_k'}\frac{\partial u_i}{\partial x_k}\right) \tag{8}$$

$$\Phi_{ij} = \overline{P'\left(\frac{\partial u_i'}{\partial x_j} + \frac{\partial u_j'}{\partial x_i}\right)} \tag{9}$$

$$\varepsilon_{ij} = -2\mu\overline{\frac{\partial u_i'}{\partial x_k}\frac{\partial u_i'}{\partial x_k}} \tag{16}$$

For computational stability, the equations for $D_{T,ij}$, $\Phi_{T,ij}$ and $\varepsilon_{T,ij}$ are modified as follows;

$$D_{T,ij} = \frac{\partial}{\partial x_k}\left(\frac{\mu_t}{\sigma_k}\frac{\partial\overline{u_i' u_j'}}{\partial x_k}\right) \tag{11}$$

where $\sigma_k = 0.82$ and μ_t is the turbulent viscosity,

$$\phi_{ij} = \phi_{ij,1} + \phi_{ij,2} + \phi_{ij,w} \tag{12}$$

with $\phi_{ij,w}$, $\phi_{ij,1}$ and $\phi_{ij,2}$ are respectively the surface reflection term, slow term, and the rapid term, where the last two are defined as

$$\phi_{ij,1} = -C_1\rho\frac{\varepsilon}{k}\left(\overline{u_i' u_j'} - \frac{2}{3}\delta_{ij}k\right) \tag{13}$$

$$\phi_{ij,2} = -C_2\left(P_{ij} - \tfrac{2}{3}P\,\delta_{ij}\right) \tag{14}$$

where C_1=1.8 and C_2=0.6.
The viscosity dissipation is related to the large-scale vortex which is essentially engaged in the transport momentum. Nevertheless, it was considered that the dissipation only occurs in small-scale isotropic vortex. So the equation for $\varepsilon_{i,j}$ is reduced to

$$\varepsilon_{ij} = \frac{2}{3}\rho\varepsilon\,\delta_{ij} \tag{15}$$

III. SIMPLIFYING ASSUMPTIONS USED IN THE TURBULENT FLOW ANALYSIS

The equations of continuity and Navier-Stokes as well as the governing equations describing the thermal convection simultaneously constitute a system of partial differential equations very complex to solve. The solutions to these complex equations are only possible for relatively simple cases. Numerical solutions would require large computer resources which are prohibitively complex and expensive. Thus to use these equations, some practical assumptions had to be made. For the case of flow inside a duct, it can be assumed that the flow is fully developed.
Basically, this means that it can be assumed that certain properties of the flow do not change with distance along the duct, which applies to real duct flows well away from the entrance or fittings. The fluid properties are also assumed to constant, and the form and profile of the velocity and temperature does not change with distance along the duct as in Fig. 1. Then the velocity and temperature profiles can be expressed in the form where the functions f and g are independent of the distance along the duct.

$$\left(\frac{u}{u_c}\right) = f\left(\frac{r}{D}\right), \qquad \left(\frac{T - T_c}{T_\omega - T_c}\right) = g\left(\frac{r}{D}\right) \tag{10}$$

International Journal of Engineering Applied Sciences and Technology, 2018
Vol. 3, Issue 4, ISSN No. 2455-2143, Pages 1-13
Published Online August 2018 in IJEAST (http://www.ijeast.com)

These simplifications mean that the velocity and temperature of the fluid at any radial distance *y* from the center line of the duct will remain constant along the duct. The wall temperature $(T - T_c)/(T_\omega - T_c)$ also remains constant. Since *u* is not changing, this implies that along the tangential and radial directions, the velocity components will be quite negligible.

$$\bar{u}\frac{\partial \bar{T}}{\partial z} + \bar{v}\frac{\partial \bar{T}}{\partial r} = \frac{1}{r}\frac{\partial}{\partial r}\left[r(\epsilon_H + \alpha)\frac{\partial \bar{T}}{\partial r}\right] \quad (17)$$

The radial velocity component ($\bar{v}$) is zero as explained before. The energy equation describing the thermal problem is then given by the following form:

$$\bar{u}\frac{\partial \bar{T}}{\partial z} = \frac{1}{r}\frac{\partial}{\partial r}\left[r(\epsilon_H + \alpha)\frac{\partial \bar{T}}{\partial r}\right] \quad (18)$$

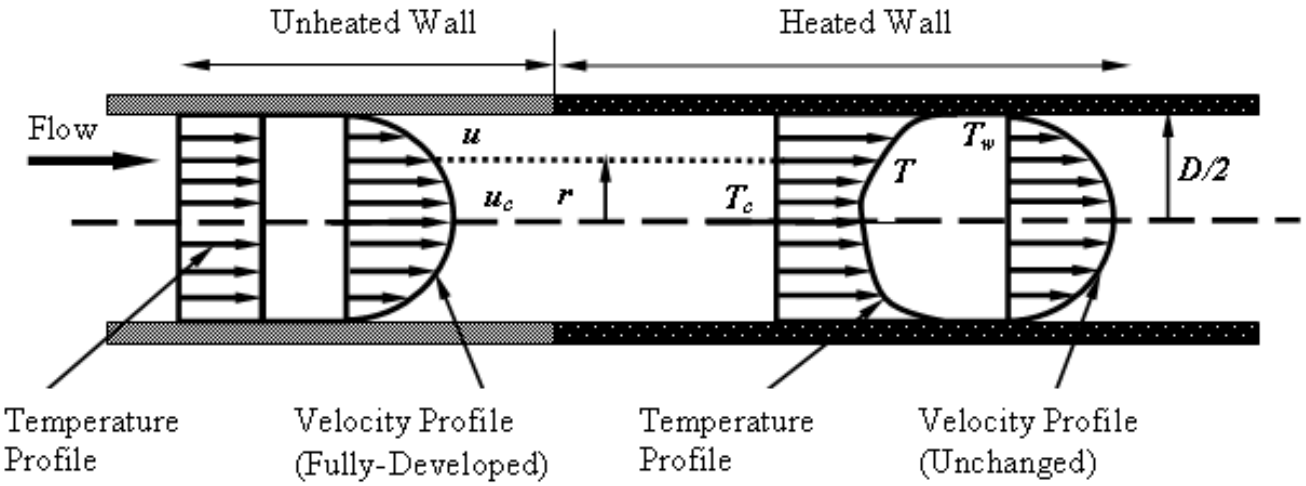

Fig. 1. Thermally developing pipe flow

III. NUMERICAL PROCEDURE OF THE THERMAL PROBLEM

A. Thermally developing pipe flow

We are interested here in a thermal problem with an initially unheated section flow inside a long pipe. The flow is fully developed before the beginning of the heating phase, in which the unheated section is considered sufficiently long. The temperature field only develops when heating begins, but the properties of the fluid are initially assumed to be constant (Wilcox, 1998). Thus, the velocity field will not vary in this region. Figure 1 clearly shows the scheme of the flow considered in this analysis.

In our simulation, we will limit the thermal problem to the case of constant fluid properties, such that the corresponding equation for turbulent flow in the tube is given as (Kays and Crawford, 1993):

The used form of the governing equations is quite parabolic while neglecting the longitudinal heat flux and considering only the radial flux. The mean velocity, $\bar{u}$, is independent of z and varies according to r. We can write the equation (18) like this

$$\bar{u}\frac{\partial \bar{T}}{\partial z} = \frac{1}{r}\frac{\partial}{\partial r}\left[r\left(\frac{\epsilon}{Pr_T} + \frac{\upsilon}{Pr}\right)\frac{\partial \bar{T}}{\partial r}\right] \quad (19)$$

The initial and boundary conditions on the solution to this equation are:

When z = 0 , $\bar{T} = T_i$

When *r* = *D*/2 , $\bar{T} = T_\omega$

When *r* = 0 , $\frac{\partial T}{\partial r} = 0$

C. Derivation of dimensionless formulas

International Journal of Engineering Applied Sciences and Technology, 2018
Vol. 3, Issue 4, ISSN No. 2455-2143, Pages 1-13
Published Online August 2018 in IJEAST (http://www.ijeast.com)

For simplification purposes, it is important to convert this equation to a dimensionless form in order to solve the problem. For this reason, we will use the following variables:

$$R = \frac{r}{D}\ , U = \frac{\bar{u}}{\bar{u}_m}\ , E = \frac{\epsilon}{\upsilon}\ , Z = \frac{z/D}{Re_D Pr} \qquad (20)$$

Where Re_D is the Raynolds as a of the average velocity $\bar{u}_m$ through a tube of diameter *D*, is defined by

$$Re_D = \frac{\bar{u}_m D}{\upsilon} \qquad (21)$$

The wall temperature is considered uniform and equal to T_ω. The dimensionless temperature is defined as follows

$$\theta = \frac{\bar{T} - T_i}{T_\omega - T_i} \qquad (22)$$

where T_i is the initial fluid temperature before the heating is triggered. The substitution of dimensionless variables into equation (19), gives

$$U\frac{\partial\theta}{\partial Z} = \frac{1}{R}\frac{\partial}{\partial R}\left[R\left(E\frac{Pr}{Pr_T} + 1\right)\frac{\partial\theta}{\partial R}\right] \qquad (23)$$

For our problem, we will obtain the following boundary and initial conditions

$$Z = 0 : \theta = 0\ , R = 0.5 : \theta = 1\ , R = 0 : \frac{\partial\theta}{\partial R} = (\qquad (24)$$

D. The Thomas algorithm

The tridiagonal matrix Thomas Algorithm is used for the resolution of a tridiagonal matrix using a method that was first developed by Llevellyn Thomas that bears his name, to solve tridiagonal system equations implicitly. The method solves a tridiagonal matrix system of the form MU = D, where M is a matrix of dimensions *N*×*N*. That is to say a matrix whose elements are null except on the three main diagonals like

$$\begin{pmatrix} b_1 & c_1 & & & & & \\ a_2 & b_2 & c_2 & & & & \\ & a_3 & b_3 & c_3 & & 0 & \\ & & \ddots & \ddots & \ddots & & \\ & & & \ddots & \ddots & \ddots & \\ & & 0 & & \ddots & \ddots & \ddots \\ & & & & \ddots & \ddots & c_{N-1} \\ & & & & & a_N & b_N \end{pmatrix} \qquad (25)$$

.The vectors U and D, of dimension N, are written:

$$U = \begin{pmatrix} u_1 \\ u_2 \\ u_3 \\ \vdots \\ \vdots \\ \vdots \\ u_{N-1} \\ u_N \end{pmatrix} \quad \text{and} \quad D = \begin{pmatrix} d_1 \\ d_2 \\ d_3 \\ \vdots \\ \vdots \\ \vdots \\ d_{N-1} \\ d_N \end{pmatrix} \qquad (26)$$

In this algorithm, we first calculate the following coefficients:

$$c_1' = \frac{c_1}{b_1} \qquad (27)$$

$$c_i' = \frac{c_i}{b_i - a_i c_{i-1}'} \quad \text{for } i = 2,3,\cdots,N-1 \qquad (28)$$

and

$$d_1' = \frac{d_1}{b_1} \qquad (29)$$

$$d_i' = \frac{d_i - a_i d_{i-1}'}{b_i - a_i c_{i-1}'} \quad \text{for } i = 1,2,\cdots,N \qquad (30)$$

The unknowns u_1 , u_2, …., u_N are then obtained by the formulas:

$$u_N = d_N' \qquad (31)$$

$$u_i = d_i' - c_i' u_{i+1} \quad \text{for } i = N-1, N-2, \ldots\ldots, 2\ , \qquad (32)$$

In CFD solution techniques, the algorithm is directly coded in the resolution process, in contrast to machine-optimized subroutines that are used on a specific computer. A simple example of a FORTRAN program to adapt this algorithm is well illustrated in Figure 2.

```
C ************************************************************
C
      SUBROUTINE TRISOL(A,B,C,D,H,N)
C
C ************** TRI-DIAGONAL MATRIX SOLVER *******************
C
C *** THIS TRIDIAGONAL MATRIX SOLVER USES THE THOMAS ALGORITHM ********
C
      dimension A(250),B(250),C(250),D(250),H(250),W(250),R(250),G(250)
      W(1)=A(1)
      G(1)=D(1)/W(1)
      do 100 I=2,N
      I1=I-1
      R(I1)=B(I1)/W(I1)
      W(I)=A(I)-C(I)*R(I1)
      G(I)=(D(I)-C(I)*G(I1))/W(I)
  100 continue
      H(N)=G(N)
      N1=N-1
      do 200 I=1,N1
      II=N-I
      H(II)=G(II)-R(II)*H(II+1)
  200 continue
      return
      end
```

Fig. 2. Subroutine for Thomas Algorithm written in FORTRAN 95.

International Journal of Engineering Applied Sciences and Technology, 2018
Vol. 3, Issue 4, ISSN No. 2455-2143, Pages 1-13
Published Online August 2018 in IJEAST (http://www.ijeast.com)

E. ***The numerical method***

Notice that the variations of the quantities U and E with R are known, as long as the fluid velocity is fully developed. The equation obtained will now be processed numerically by the finite difference method since it is better adapted to a medium with a wall temperature that varies according to the longitudinal coordinate Z. This method is simple in its concept but effective in its results, as such it is often used in heat transfer problems.

Figure 3 represents the nodal points used in the numerical simulation. Here the finite difference method of approximations is introduced and an explicit backward order of order 1 in the direction (i) is used where the variable U does not change, to evaluate values at the spatial coordinate (Z).

$$U \left.\frac{\partial \theta}{\partial Z}\right|_{i,j} = U_j \left[\frac{\theta_{i,j} - \theta_{i-1,j}}{\Delta Z}\right] \tag{33}$$

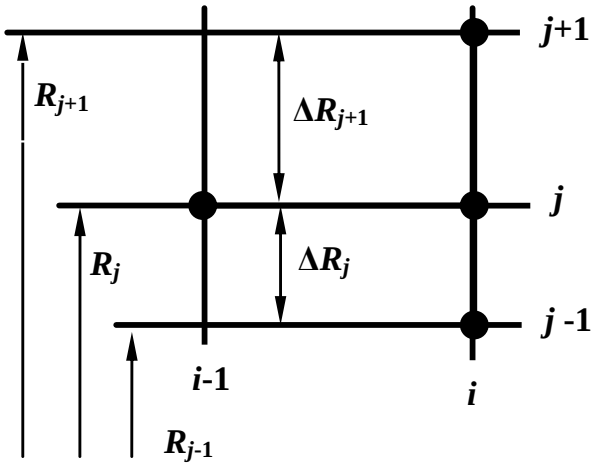

Fig. 3. Nodal points used in obtaining finite-difference solution

$$\frac{1}{R}\frac{\partial}{\partial R}\left[R\left(E\frac{Pr}{Pr_T}+1\right)\frac{\partial \theta}{\partial R}\right]\Big|_{i,j} = \frac{1}{R_j}\frac{2}{\Delta R_{j+1}+R_j} \tag{34}$$
$$\left\{\left[\frac{R_{j+1}\left(E_{j+1}\,Pr/Pr_T+1\right)+R_j\left(E_j\,Pr/Pr_T+1\right)}{2}\right]\left(\frac{\theta_{i,j+1}-\theta_{i,j}}{\Delta R_{j+1}}\right)-\left[\frac{R_j\left(E_j\,Pr/Pr_T+1\right)+R_{j-1}\left(E_{j-1}\,Pr/Pr_T+1\right)}{2}\right]\left(\frac{\theta_{i,j}-\theta_{i,j-1}}{\Delta R_j}\right)\right\}$$

By replacing the derivatives by its finite difference approximations obtained from equation (23), we obtain an equation in the following form:

$$A_j\theta_{i,j} + B_j\theta_{i,j+1} + C_j\theta_{i,j-1} = D_j \tag{35}$$

The coefficients A_j, B_j, C_j and D_j resulting from the calculations are obtained from the mining form

$$A_j = \frac{U_j}{\Delta Z} + \frac{1}{R_j}\frac{2}{\Delta R_{j+1}+\Delta R_j} \tag{36}$$
$$\left\{\left[\frac{R_{j+1}\left(E_{j+1}\,Pr/Pr_T+1\right)+R_j\left(E_j\,Pr/Pr_T+1\right)}{2}\right]\left(\frac{1}{\Delta R_{j+1}}\right)+\left[\frac{R_j\left(E_j\,Pr/Pr_T+1\right)+R_{j-1}\left(E_{j-1}\,Pr/Pr_T+1\right)}{2}\right]\left(\frac{1}{\Delta R_j}\right)\right\}$$

$$B_j = -\frac{1}{R_j}\frac{2}{\Delta R_{j+1}+\Delta R_j} \tag{37}$$
$$\left\{\left[\frac{R_{j+1}\left(E_{j+1}\,Pr/Pr_T+1\right)+R_j\left(E_j\,Pr/Pr_T+1\right)}{2}\right]\left(\frac{1}{\Delta R_{j+1}}\right)\right\}$$

$$C_j = -\frac{1}{R_j}\frac{2}{\Delta R_{j+1}+\Delta R_j} \tag{38}$$
$$\left\{\left[\frac{R_j\left(E_j\,Pr/Pr_T+1\right)+R_{j-1}\left(E_{j-1}\,Pr/Pr_T+1\right)}{2}\right]\left(\frac{1}{\Delta R_j}\right)\right\}$$

$$D_j = \frac{U_j\theta_{i-1,j}}{\Delta Z} \tag{39}$$

Insertion of boundary conditions of the problem leads us to $\theta_{i,2} = \theta_{i,1}$ and $\theta_{i,N} = 1$. By exploiting boundary conditions while applying all "internal" points (j = 2.3, ..., N-2, N-1) in equation Eq. (35). We get a system of N equations for N unknowns θ summarized from the following form

$$\begin{aligned}
&\theta_{i,1} - \theta_{i,2} = 0\\
&A_2\theta_{i,2} + B_2\theta_{i,3} + C_2\theta_{i,1} = D_2\\
&A_3\theta_{i,3} + B_3\theta_{i,4} + C_3\theta_{i,2} = D_3\\
&A_4\theta_{i,4} + B_4\theta_{i,5} + C_4\theta_{i,3} = D_4\\
&\vdots\\
&A_{N-1}\theta_{i,N-1} + B_{N-1}\theta_{i,N} + C_{N-1}\theta_{i,N-2} = D_{N-1}\\
&\theta_{i,N} = 1
\end{aligned} \tag{40}$$

Or in matrix form

$$\begin{bmatrix}
1 & -1 & 0 & 0 & 0 & \dots & 0 & 0 & 0\\
C_2 & A_2 & B_2 & 0 & 0 & \dots & 0 & 0 & 0\\
0 & C_3 & A_3 & B_3 & 0 & \dots & 0 & 0 & 0\\
0 & 0 & C_4 & A_4 & B_4 & \dots & 0 & 0 & 0\\
\vdots & \vdots & \vdots & \vdots & \vdots & \ddots & \vdots & \vdots & \vdots\\
0 & 0 & 0 & 0 & 0 & \dots & C_{N-1} & A_{N-1} & B_{N-1}\\
0 & 0 & 0 & 0 & 0 & \dots & 0 & 0 & 0
\end{bmatrix}
\begin{bmatrix}
\theta_{i,1}\\ \theta_{i,2}\\ \theta_{i,3}\\ \theta_{i,4}\\ \vdots\\ \theta_{i,N-1}\\ \theta_{i,N}
\end{bmatrix}
=
\begin{bmatrix}
0\\ D_2\\ D_3\\ D_4\\ \vdots\\ D_{N-1}\\ 1
\end{bmatrix} \tag{41}$$

$$Q\,\theta_{i,j} = R \tag{42}$$

where Q is a tridiagonal matrix. This can be effectively solved by Thomas's algorithm for tridiagonal matrix.

For any value of Z, we can estimate the local heat transfer rate as follows:

$$q_\omega = k \left.\frac{\partial \bar{T}}{\partial r}\right|_{r=R} \tag{43}$$

International Journal of Engineering Applied Sciences and Technology, 2018
Vol. 3, Issue 4, ISSN No. 2455-2143, Pages 1-13
Published Online August 2018 in IJEAST (http://www.ijeast.com)

from where

$$\frac{q_\omega D}{k(T_\omega - T_i)} = \left.\frac{\partial\theta}{\partial R}\right|_{R=0.5} \quad (44)$$

which implies

$$Nu_{iD} = \left.\frac{\partial\theta}{\partial R}\right|_{R=0.5} \quad (45)$$

where Nu_{iD} is the local Nusselt number, then

$$Nu_{iD} = \frac{q_\omega D}{k(T_\omega - T_i)} \quad (46)$$

However

$$\left.\frac{\partial\theta}{\partial R}\right|_{i,1} = \frac{\theta_{i,N} - \theta_{1,N-1}}{\Delta R_N} \quad (47)$$

Then replacing equation (47) into equation (45) gives

$$Nu_{iD} = \frac{\theta_{i,N} - \theta_{1,N-1}}{\Delta R_N} \quad (48)$$

This Nusselt number is based on the spacing between wall temperatures and local average temperatures, the flow via the pipe is practically considered, so we draw

$$Nu_D = \frac{q_\omega D}{k(T_\omega - \bar{T}_m)} = \frac{q_\omega D}{k} Nu \quad (49)$$

where *Nu* is the averaged local Nusselt number. This can be expressed as; $Nu = \frac{1}{T_\omega - \bar{T}_m}$.

Substituting the previous equation (46) into equation (49), allows us to write

$$Nu_D = Nu_{iD}\frac{T_\omega - T_i}{T_\omega - \bar{T}_m} = \frac{Nu_{iD}}{\theta_m} \quad (50)$$

with

$$\theta_m = \frac{T_\omega - \bar{T}_m}{T_\omega - T_i} \quad (51)$$

We can then define the bulk temperature through the tube which is the temperature of the fluid that can be calculated by

$$T_b = \frac{\int_0^{D/2} \rho 2\pi r dr \bar{u} c_p \bar{T}}{\int_0^{D/2} \rho 2\pi r dr \bar{u} c_p} \quad (52)$$

In this expression, the denominator indicates the multiplication of the specific heat integrated in the flow zone and the mass flow while the numerator indicates the total energy flowing through the tube. This results in the following expression

$$\bar{T}_m = \frac{\int_0^{D/2} \bar{u}\bar{T} r dr}{\int_0^{D/2} \bar{u} r dr} \quad (53)$$

which can be written as

$$\theta_m = \int_0^{0.5} U\,\theta\, RdR \Big/ \int_0^{0.5} U\, RdR \quad (54)$$

By using the pre-determined numeric value of θ with *R* for any value of *Z*, the values θ_m can be drawn. So, we can determine the value of Nu_D at this value of *Z*,

The solution to this problem can then be obtained such that, we must specify the variations of *U* and *E*= (ϵ/υ) in which the distribution of *E* is given by the following equations

$$\begin{aligned} y^+ < 5 &: E = 0 \\ 5 \le y^+ \le 30 &: E = \frac{y^+}{5} - 1 \\ y^+ > 30 &: E = 1.6R(y^+)^{6/7} - 1 \end{aligned} \quad (55)$$

with

$$y^+ = \frac{y}{\upsilon}\sqrt{\frac{\tau_\omega}{\rho}} = (0.5 - R)Re_D\sqrt{\frac{f}{8}} \quad (56)$$

in which *f* is the friction factor

$$f = \frac{0.305}{Re_D{}^{0.25}} \quad (57)$$

This is valid for hydraulically smooth pipe with turbulent flow, up to the Reynolds number 10^5 ($Re < 10^5$),

$$\frac{\bar{u}}{\bar{u}_c} = \left(\frac{D - 2r}{D}\right)^{1/7} \quad (58)$$

The distribution of the average speed is presumed to be appreciable as follows. Where $\bar{u}_c$ means the center line speed. Now the value of $\bar{u}_m$ becomes

$$\bar{u}_m = \frac{8}{D^2}\int_0^{D/2} \bar{u} r dr \quad (59)$$

which tends towards

$$\frac{\bar{u}_m}{\bar{u}_c} = 8\int_0^{0.25} (1 - 2R)^{1/7} RdR = \frac{49}{60} \quad (60)$$

By comparing the two equations, we can draw the following result

$$U = \frac{49}{60}(1 - 2R)^{1/7} \quad (61)$$

This equation finally gives us the variation of the average dimensionless velocity *U* as a function of the radius of tube *R*. FORTRAN 95 program was used to solve the thermal values in a fully developed turbulent flow inside a cylindrical tube with uniform wall temperature, using the finite difference method.

International Journal of Engineering Applied Sciences and Technology, 2018
Vol. 3, Issue 4, ISSN No. 2455-2143, Pages 1-13
Published Online August 2018 in IJEAST (http://www.ijeast.com)

IV. RESULTS AND DISCUSSION

A. *Uniform wall temperature*

Figure 4 illustrates the variation in dimensionless temperature derivatives in the thermal entrance region for *Pr*=0.7 for various values of Re_D, with a uniform wall temperature with respect to radius, for different Reynolds number, Re_D in the thermal development region. Notice that in the fully developed zone, the behavior of the values is related to the Reynolds number whose correlation becomes very noticeable as the analysis advances into the thermal input region. This significant change is due to the high friction near the entrance to the pipe.

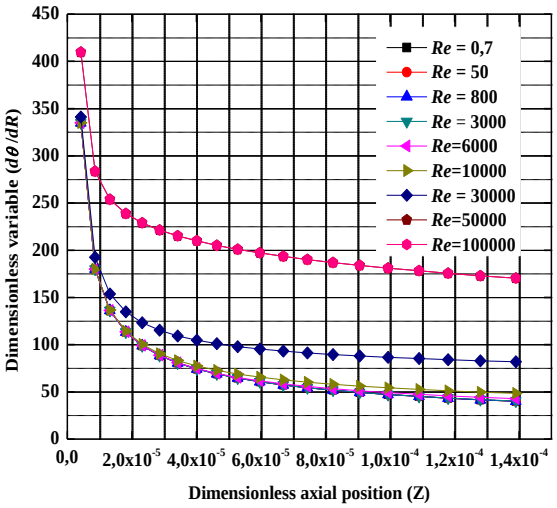

Fig. 4. Variation of dimensionless temperature derivative ($d\theta/dR$) in thermal entrance region for *Pr*=0.7 for various values of Re_D

The average Nusselt number Nu_D along the pipe is shown in Figure 5 for different Reynolds number Re_D at Prandlt number Pr=0.7. The Nu number helps to determine whether the flow is hydrodynamically fully developed, or otherwise. The decrease in Nu for Re=100000 to 50000 is very significant such that it is suggest different flow regimes occurred at these two Reynolds number values. There is also a high gradient of Nu changes for axial positions near the entrance to the tube. This high gradients are caused by high friction in the flow near the entrance to the pipe.

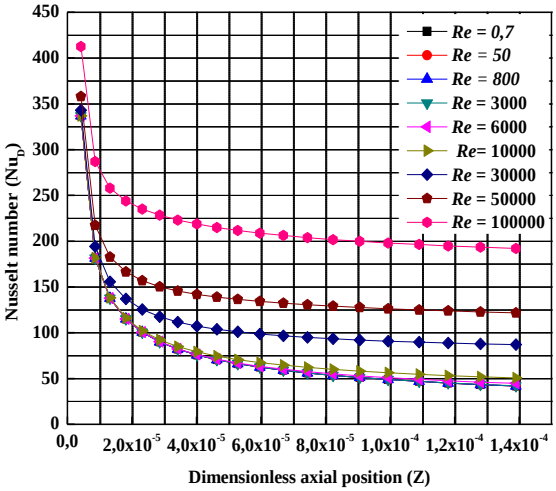

Fig.5. Variation of Nusselt number Nu_D in the thermal entrance region for *Pr*=0.7 and various values of Re_D

Using the results obtained from the calculation codes, the values of the Nusselt number for various values of the Prandtl number was plotted against the pipe axial position as shown in Figure 6. With approximate distances from the tube entrance, it has been found that the Prandtl number has a much greater effect on the Nusselt number values. In fact, although it is hard to see in the presented scale, different Prandtl values also yielded different Nu values for the isothermal wall condition.

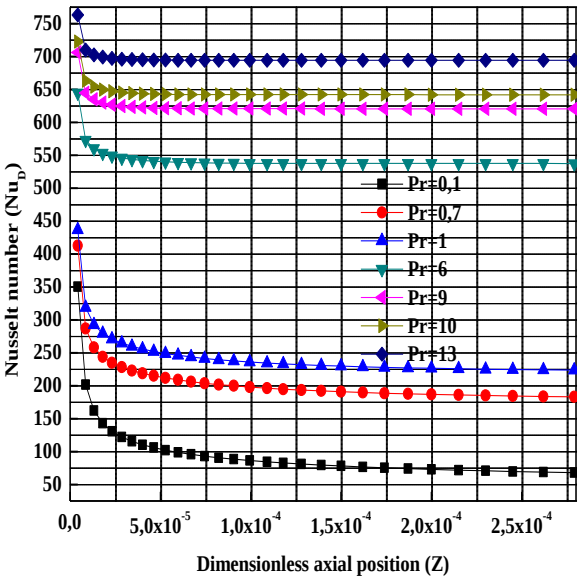

Fig.6. Variation of Nusselt number Nu_D in the thermal entrance region for $Re_D = 10^5$ for various values of *Pr*

International Journal of Engineering Applied Sciences and Technology, 2018
Vol. 3, Issue 4, ISSN No. 2455-2143, Pages 1-13
Published Online August 2018 in IJEAST (http://www.ijeast.com)

The maximum Nusselt number versus Reynolds number was plotted in Figure 7 for the constant wall temperature case. The results were calculated and plotted for Peclet numbers 0.7, 1, 6, 9, 10, and 13 to see how the Peclet number affects the Nusselt number distribution in the flow. The more the Peclet number increases, the more the Nusselt number increases with the increase of the Reynolds number which characterizes the flow. At Pe= 0, 7, the difference is perfectly very small, and at higher Peclet numbers, the difference is still large and significant.

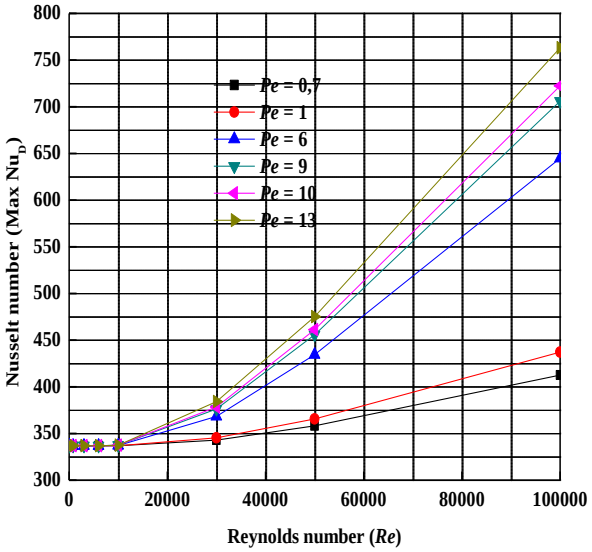

Fig.7. Variation of Nusselt number Nu_D versus Reynolds number for various values of *Pe*

The dimensionless temperature was plotted at dimensionless radial positions for the constant wall temperature case. The results were calculated and plotted for Reynolds numbers 50, 800, 3000, and 6000 and are presented in Figure 8. Figure 8 shows that when the Reynolds number is low, the temperature of the fluid varied markedly from the centre of the tube (equal to the inlet temperature) to the wall. This variation reduces as the Re is increased, to equal the wall temperature when as Re reaches 3000. Re being the ratio of inertial to frictional forces related to the viscosity of the fluid, would increase gradually as the temperature of the heating fluid increases gradually from the inlet values to the wall temperature.

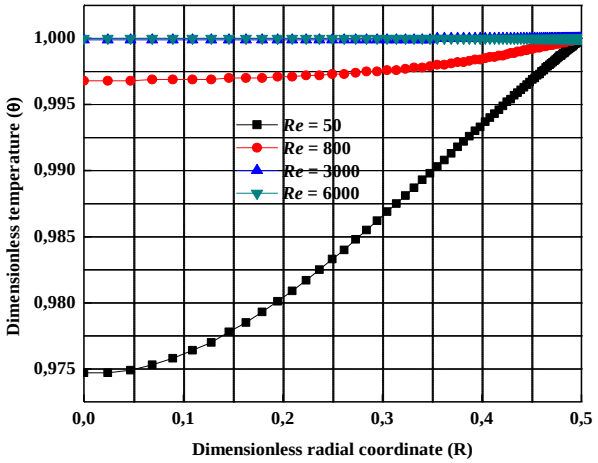

Fig.8. Dimensionless temperature profile (θ) along radial coordinate for different values of Reynolds number.

The dimensionless axial velocity profile, as a function of radial position for turbulent flow at Prandtl number Pr= 0.7 is depicted in Figure 9. Fully developed laminar flow would produce the parabolic profile, while a turbulent flow would produce a much steeper slope near the wall. The axial velocity is maximum at the centerline and gradually decreases at the wall to satisfy the no-slip boundary condition for viscous flow. The figure shows that the effect of rotation in the turbulent pipe flow at the exit. The pipe rotation influences the mean stream wise velocity component such that the maximum velocity in the center of the pipe increases while the velocity close to the wall decreases. This effect results in a slight decrease of the shear stresses at the wall and an overall decrease of the pressure-drop.

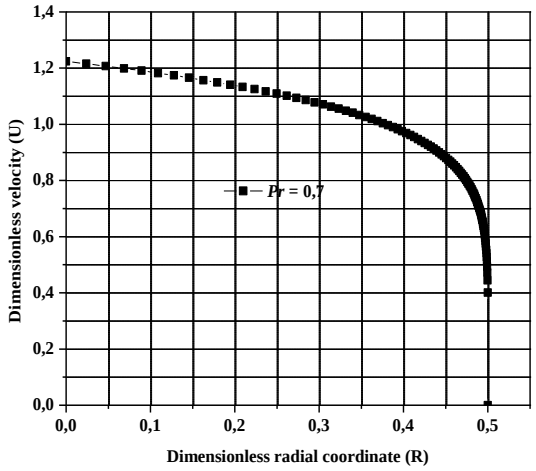

Fig. 9. Dimensionless axial velocity profile (U) for Pr=0.7

International Journal of Engineering Applied Sciences and Technology, 2018
Vol. 3, Issue 4, ISSN No. 2455-2143, Pages 1-13
Published Online August 2018 in IJEAST (http://www.ijeast.com)

The dimensionless eddy viscosity distribution (E) along the dimensionless radius of the pipe at different values of the Reynolds numbers (Re) is shown in Figure 10. It can be seen that the dimensionless eddy viscosity profiles also have a more uniform and almost parabolic symmetric distribution whose concavity of this parabola is variable according to the Reynolds number. We see a significant change in maximum eddy viscosity towards the central part of the pipe at Reynolds number values above 6000, where the turbulent regime begins in the pipe (Re>4000). Indeed, turbulent flow consists of eddies of various size ranges, which increase with increasing Reynolds number. The kinetic energy of the flow would cascade down from large to small eddies of interactional forces between the eddies.

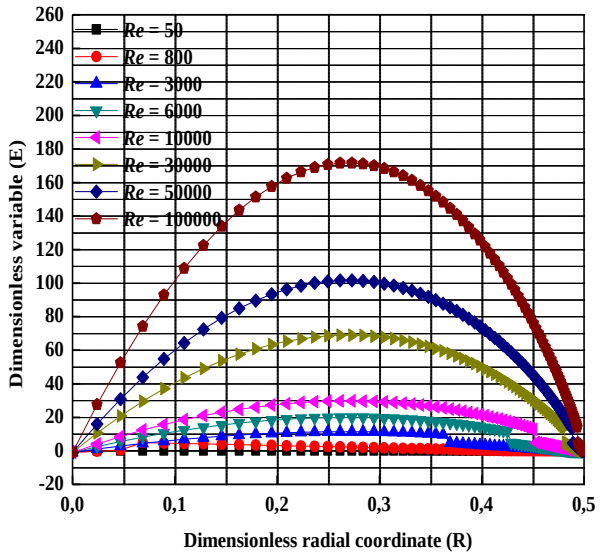

Fig. 10. Dimensionless eddy viscosity distribution (E) along the dimensionless radius (R) at P_r=0.7 for various Reynolds numbers of the flow.

B. Wall heat flux uniform

Fig. 11 shows the Nusselt number variations at the thermal entrance region for Pr=0.7 plotted for different values of Re_D in the case of uniform wall heat flux, in order to represent the augmentation in the heat transfer. It can be seen that as Re increases above 10,000 the average Nusselt number for the circular tube starts to increase significantly. Axially the Nu values decreased rapidly from the entrance to a point of about $Z=5 \times 10^{-5}$, after which the reduction is of lower and constant values as shown with the straight line graphs. The straight lines also show that the turbulent flow is fully developed. The development of the turbulent flow is significantly affected by the large Reynolds number values.

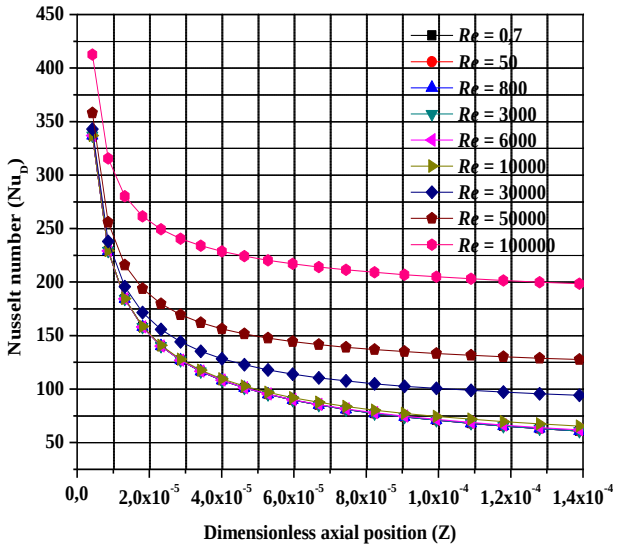

Fig.11. Variation of Nusselt number Nu_D in thermal entrance region for Pr=0.7 for various values of Re_D

Nusselt number Nu_D variations with axial variations at Reynolds number 6000 and Prandtl number 0.7 as obtained from the program codes for fully developed turbulent flow in the tube with constant wall heat flux are shown in Table 1.

Table 1. Summarized results of the FORTRAN 95 code for uniform wall heat flux for Re =6000 and Pr=0.7

Z	T_{Wall}	Nu_{Di}	Nu_{Da}
0,0000042	0,0030	334,9473	336,8423
0,0000086	0,0044	227,3414	229,1351
0,0000132	0,0055	182,6194	184,4026
0,0000181	0,0064	156,3688	158,1592
0,0000232	0,0072	138,4781	140,2811
0,0000286	0,0080	125,2165	127,0338
0,0000342	0,0087	114,8419	116,6743
0,0000401	0,0094	106,4161	108,2639
0,0000463	0,0101	99,3814	101,245
0,0000528	0,0107	93,3841	95,2636
0,0000597	0,0113	88,1857	90,0813
0,0000669	0,012	83,6188	85,5309
0,0000744	0,0126	79,5622	81,4912
0,0000823	0,0132	75,9255	77,8718
0,0000906	0,0138	72,6394	74,6036
0,0000994	0,0144	69,6501	71,6326

International Journal of Engineering Applied Sciences and Technology, 2018
Vol. 3, Issue 4, ISSN No. 2455-2143, Pages 1-13
Published Online August 2018 in IJEAST (http://www.ijeast.com)

0,0001085	0,0149	66,915	68,9166
0,0001182	0,0155	64,3988	66,42
0,0001283	0,0161	62,0737	64,1152
0,0001389	0,0167	59,9168	61,9793
0,0001500	0,0173	57,9081	59,9923

J	*R*	*U*	*T*	*E*
1	-0,0000003	1,224	0,788	-1
2	0,024	1,216	0,788	2,471
3	0,04686	1,207	0,7884	5,496
4	0,06863	1,199	0,7889	8,121
5	0,08936	1,191	0,7893	10,39
6	0,1091	1,182	0,7898	12,33
7	0,1279	1,174	0,7903	13,98
8	0,1458	1,166	0,7907	15,37
9	0,1629	1,157	0,7912	16,52
10	0,1791	1,149	0,7917	17,47
11	0,1946	1,141	0,7921	18,24
12	0,2093	1,133	0,7926	18,83
13	0,2234	1,125	0,793	19,28
14	0,2367	1,117	0,7935	19,6
15	0,2495	1,109	0,7939	19,81
16	0,2616	1,102	0,7943	19,91
17	0,2731	1,094	0,7948	19,93
18	0,2841	1,086	0,7952	19,86
19	0,2946	1,078	0,7956	19,73
20	0,3046	1,071	0,796	19,53
21	0,3141	1,063	0,7964	19,29

The dimensionless temperature profiles along the dimensionless radius are plotted in Figure 12 for a single value of the Prandtl number (0.7) and various Reynolds numbers. Note that the effects of increasing the Reynolds number is to give a more "square" temperature profile, while a low Reynolds number yields a more rounded profile that is similar to that for laminar flow. Still higher and lower values of Reynolds number continue these trends. Note that as the Reynolds becomes higher than 3,000 the dimensionless temperature approaches a constant value along the radius approaching the threshold of 0.80.

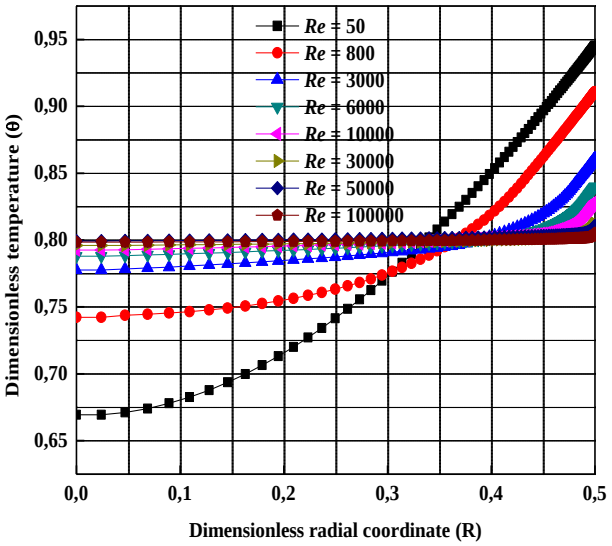

Fig.12. Temperature behavior (θ) versus dimensionless radius (R) for various values of Reynolds number

The dimensionless eddy viscosity distribution E as a function of dimensionless axial position plotted for one particular value of the Prandtl number in Figure 13 at different Re numbers. As can be seen in this Figure, the surface temperature increases from a certain value at the pipe center with the increasing of the Reynolds number Re. Note that the eddy diffusivity is maximum at the tube centerline. Indeed, the relative viscosity increases from the pipe wall towards the pipe centre because the fluid tends to behave like a solid rather than a liquid when approaching the core region of the pipe, due to the lower shear rate in this region. That is why the dimensionless Eddy viscosity, is related to the dimensionless shear rate and the Reynolds number.

International Journal of Engineering Applied Sciences and Technology, 2018
Vol. 3, Issue 4, ISSN No. 2455-2143, Pages 1-13
Published Online August 2018 in IJEAST (http://www.ijeast.com)

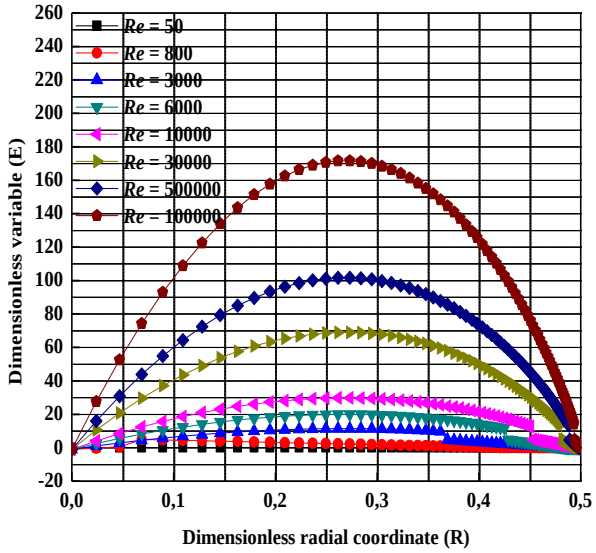

Fig.13. Dimensionless eddy viscosity distributions (*E*) versus dimensionless radius (*R*) for various Reynolds number

C.Comparison of constant wall temperature and heat flux cases

For the calculations of the heat transfer in a fully developed turbulent flow inside a circular pipe, we will compare the current numerical Nusselt numbers results for the case of constant wall temperature and the case of constant heat flux at constant Reynolds number of 10^4 (shown in Figure 14) and for constant Prandtl number of 0.7 (shown in Figure 15). It can be seen that the Nusselt number in the case of uniform wall temperature lie above the numbers for wall in uniform heat flux. This Nu values decreased sharply exponentially at the entrance but the decrease reduced to lower rate further down the pipe. But the final values for the two cases differ quite markedly in the flow far from the entrance. Similar curves were produced for constant Prandtl number (0.7) as shown Figure 15.

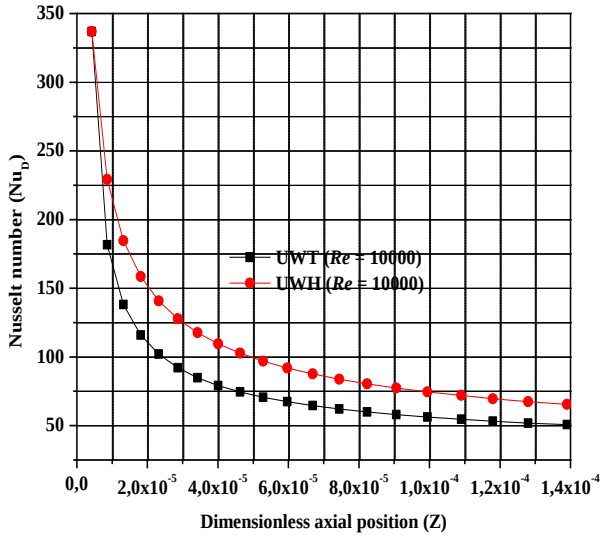

Fig .14. The Comparison of Nusselt number profile for uniform wall temperature with the uniform wall heat flux for Re =10000.

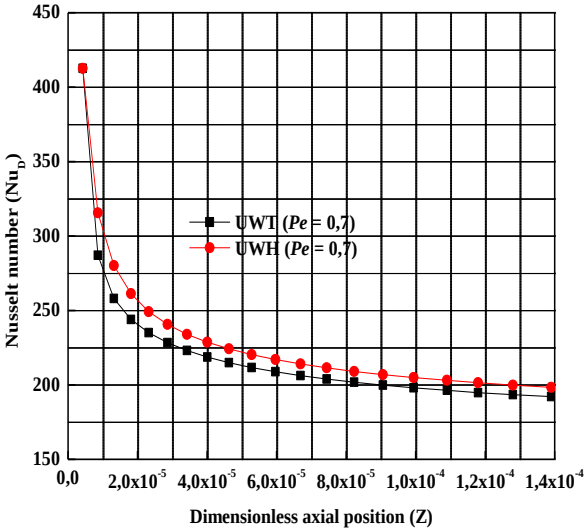

Fig.15. The Comparison of Nusselt number profile for uniform wall temperature with the uniform wall heat flux for Pr =0.7.

Figure 16 show the effects of boundary conditions (constant wall temperature. (CWT) and constant wall heat flux (CWHF)) on the dimensionless temperature in the pipe for Re=10^4. Constant heat flux and constant temperature surfaces do not give the same results (in terms of θ) when the flow becomes strongly unsteady and turbulent. Constant heat flux surfaces produce colder zones at high Re thus yielding a reduced Nu. Note that, only at very low Prandtl numbers, there would be a significant difference of temperatures between the constant-heat-rate and constant-surface temperature cases.

International Journal of Engineering Applied Sciences and Technology, 2018
Vol. 3, Issue 4, ISSN No. 2455-2143, Pages 1-13
Published Online August 2018 in IJEAST (http://www.ijeast.com)

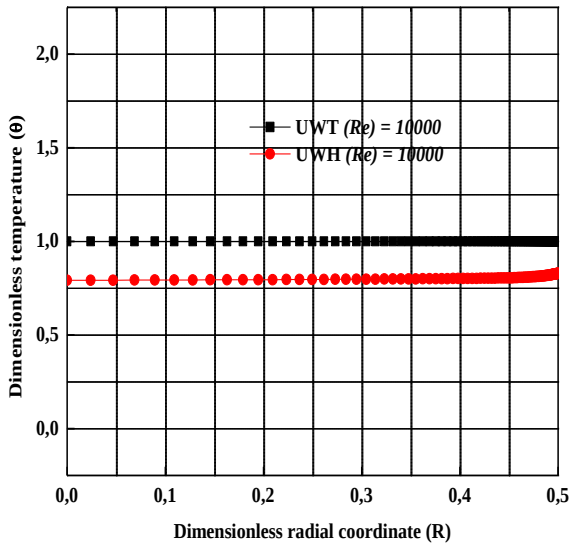

Fig. 16. Comparison of dimensionless temperature behavior in the two case for Re =10^4

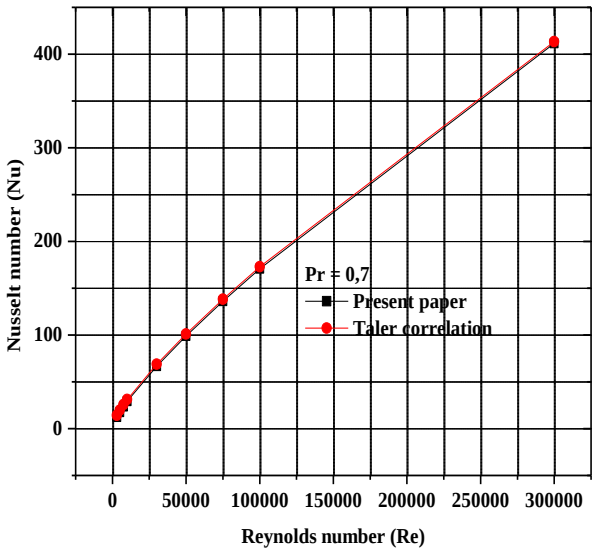

Fig. 17. Comparison of the numerical data obtained in the present work and the data from Taler (2016) for turbulent air flow in a tube with constant wall heat flux.

D. Comparison of the present numerical model and the previous correlation data

In order to verify and validate the numerical results of this simulation of the thermal problem, the results are compared to the work recently performed by Taler (2016) using the finite difference method. Taler evaluated Nusselt numbers or various Reynolds and Prandtl numbers. In addition, the Nusselt numbers were obtained for fully developed turbulent flow in tubes with constant wall heat flux after solving the energy conservation equation.

The comparison of the results of the Nusselt numbers (Nu) as a function of Reynolds number (Re) for the case of the Prandtl number (Pr = 0.7) for air flowing inside a circular heating pipe is illustrated in Fig.17. It can be observed that the numerical solutions match the work of Taler (2016) very well, with an average deviation of less than 2% for Pr=0.7. This is a very good agreement. Thus the treated thermal model has been well verified and validated and the comparison results confirm the reliability of this numerical program.

VI. CONCLUSIONS

The impact of our contribution on the prediction of the heat transfer rate at the wall of a pipe towards a fluid in turbulent flow is presented. Main attention was given to two dimensional and axi-symmetric flow through circular pipes. The methodology of the analysis is based on the thermal equations of turbulent flow models and finite-difference methods. The equations were adapted for any thermal boundary conditions, so long as the velocity profile was assumed to be fully developed at the point where heat transfer starts. A program using FORTRAN 95 simulating the fully developed turbulent fluid flow through a circular tube was developed. Then a simulation for the two thermal boundary conditions of uniform wall temperature and constant heat flux, were carried out. It was found that the surface temperature is higher for high Reynolds numbers than for low Reynolds numbers, due to the free convection domination on the combined heat transfer process. Mean axial velocity and temperature profiles were shown to increase and extend farther in the outer layer with increasing Reynolds number. This consequently made the local Nu numbers to be higher for high Re numbers than for low Re numbers. This is due to the forced convection that dominates the heat transfer process. The thermal current results in this numerical study, shows that the influence and sensitivity of some of the parameters involved in the calculations and the results of available literature agree very well, with uncertainties of less than 2%. In the fully developed turbulent flow, the Nusselt number, as well as the dimensionless temperatures increase with increasing Reynolds numbers. It is also necessary to compare

the numerical results, especially for Nusselt numbers, temperatures and velocity profile obtained in this simulation of the Navier-Stokes equations for fully developed axis-symmetric flow, with experimental data.
It should also be mentioned that the same solution procedure can be used for any dynamically developed velocity profile and turbulent model in other conduit configurations such as channel geometries and rectangular, triangular or other sections. Different wall heating conditions, and viscous and other flows could also be evaluated for different heating effects.

VII. ACKNOWLEDGEMENTS

The authors are thankful to the anonymous reviewers for their constructive feedback and criticism towards improvising the quality of this work.

VIII. REFERENCES

[1] Zhou A., Pirozzoli S., Klewicki J.(2017). Mean equation based scaling analysis of fully-developed turbulent channel flow with uniform heat generation, *International Journal of Heat and Mass Transfer*, 115(B), (pp.50-61).
[2] Wei T., Fife P., Klewicki J., McMurtry P.(2005). Scaling heat transfer in fully developed turbulent channel flow, *International Journal of Heat and Mass Transfer*, 48(25-26), (pp.5284-5296).
[3] Everts M., and Meyer J.P. (2018). Relationship between pressure drop and heat transfer of developing and fully developed flow in smooth horizontal circular tubes in the laminar, transitional, quasi-turbulent and turbulent flow regimes, *International Journal of Heat and Mass Transfer* 117, (pp.1231-1250).
[4] Everts M., and Meyer J.P.(2018). Heat transfer of developing and fully developed flow in smooth horizontal tubes in the transitional flow regime, *International Journal of Heat and Mass Transfer*,17, (pp.1331-1351).
[5] Aravinth S., (2000). Prediction of heat and mass transfer for fully developed turbulent fluid flow through tubes, *International Journal of Heat and Mass Transfer*, 43(8), (pp.1399-1408).
[6] Teitel M., and Antonia R.A.,(1993). Heat transfer in fully developed turbulent channel flow: comparison between experiment and direct numerical simulations, *International Journal of Heat and Mass Transfer*, 36(6), (pp. 1701-1706).
[7] Koizumi H.,(2002). Laminar–turbulent transition behavior of fully developed air flow in a heated horizontal tube, *International Journal of Heat and Mass Transfer*, 46(5), (pp. 937-949).
[8] Gnielinski V. ,(1976). New equations for heat and mass transfer in turbulent pipe and channel flow, *International Chemical Engineering* , 16(2), (pp. 359-368).
[9] Taler D.(2016). A new heat transfer correlation for transition and turbulent fluid flow in tubes, *International Journal of Thermal Sciences*, 108, (pp.108-122).
[10] Babadus'haq R.F. (1993). Forced Convection Heat Transfer in the Entrance Region of Pipes, *International Journal of Heat and Mass Transfer* 36(13), (pp.3343-3349).
[11] Belhocine A., and Wan Omar W.Z.(2016). Numerical study of heat convective mass transfer in a fully developed laminar flow with constant wall temperature, *Case Studies in Thermal Engineering*, 6, (pp.116-127).
[12] Belhocine A.,(2016). Numerical study of heat transfer in fully developed laminar flow inside a circular tube. *International Journal of Advanced Manufacturing Technology*, 85(9), (pp.2681–2692).
[13] Belhocine A., and Wan Omar W.Z.,(2017). An analytical method for solving exact solutions of the convective heat transfer in fully developed laminar flow through a circular tube , *Heat Transfer—Asian Research*, 46(8), (pp.1342-1353).
[14] Belhocine A., and Wan Omar W.Z.,(2018). Similarity solution and Runge Kutta method to a thermal boundary layer model at the entrance region of a circular tube, *Revista Científica*, 31(1), (pp.6-18).
[15] Bryant D.B., Sparrow E.M., Gorman J.M.,(2018). Turbulent pipe flow in the presence of centerline velocity overshoot and wall-shear undershoot, *International Journal of Thermal Sciences*, 125, (pp.218-230).
[16] Wilcox D.C.(1998). *Turbulence Modeling for CFD*, DCW Industries, La Canada, USA, 2nd ed.
[17] Kays W.M., and Crawford M.E.(1993), *Convective Heat and Mass Transfer*, McGraw-Hill, New York, 3rd Edition.